Amorphouslike Density of Gap States in Single-Crystal Pentacene

D.V. Lang,[1,2] X. Chi,[2] T. Siegrist,[3] A. M. Sergent,[3] and A. P. Ramirez[3,2]
[1]*Los Alamos National Laboratory, Los Alamos, New Mexico 87545, USA*
[2]*Columbia University, New York, New York 10027, USA*
[3]*Bell Laboratories, Lucent Technologies, 600 Mountain Avenue, Murray Hill, New Jersey 07974, USA*
(Received 4 December 2003; published 19 August 2004)

We show that optical and electrical measurements on pentacene single crystals can be used to extract the density of states in the highest occupied molecular orbital–lowest unoccupied molecular orbital band gap. It is found that these highly purified crystals possess band tails broader than those typically observed in inorganic amorphous solids. Results on field-effect transistors fabricated from similar crystals imply that the gap state density is much larger within 5–10 nm of the gate dielectric. Thus, organic thin-film transistors for such applications as flexible displays might be significantly improved by reducing these defects.

DOI: 10.1103/PhysRevLett.93.086802 PACS numbers: 85.65.+h, 72.80.Le

Organic semiconductors, such as pentacene, are promising for applications requiring large-area coverage, flexibility, low-temperature processing, and low cost [1,2]. Indeed, flexible displays based on organic thin-film transistors are near the threshold of practicality. However, there is evidence that defects and/or impurities limit maximum device performance. If the carrier mobility in organic thin-film transistors were increased 100× from today's values (typically ~ 1 cm^2/V sec), one could imagine a wide variety of electronic circuits embedded into everyday items. It is therefore important to identify the localized gap states that limit electronic transport. It is well known that the maximum time-of-flight mobility can only be obtained in ultrapurified organic crystals [3]. The effective mobility of holes in pentacene thin-film transistors (TFTs) increases with increasing crystal perfection [2], with an increased concentration of localized states 5–10 nm from the gate dielectric [4]. We previously showed that the effective mobility of single-crystal pentacene field-effect transistors (FETs) is limited by localized states near the valence band [5].

In this Letter we will show that purified pentacene single crystals have exponential band tails broader than in inorganic amorphous material. FETs fabricated from similar pentacene crystals also have broad tails of valence-band states near the gate dielectric, with 10× larger concentration than in the bulk. Thus the performance of pentacene FETs is not limited by the properties of the underlying material but by defects and/or impurities near the interface with the gate dielectric.

The pentacene crystals were grown by physical vapor transport [5], and were 10–30 mm^2 in area and 25–50 μm thick. To evaluate crystal quality, rocking curves of a sample from the same batch were obtained on a custom four-circle diffractometer with monochromated Cu-$K\alpha$ radiation. Rocking curves of (002) and (004) reflections were evaluated, and the widths indicated mosaic spreads of the order of 0.2 degrees and better. Because of the intrinsic resolution of the diffractometer further evaluation will require tighter resolution. The contacts were *e*-beam evaporated Ti (5 nm)/Au (500 nm) through a shadow mask giving an array of 400 μm-square metal pads separated by 30 μm gaps along the columns and 108 μm gaps along the rows. The measurements were made on the 30 μm gaps with a specular surface in a temperature-variable vacuum probe station using a Keithley 6517A electrometer. The photoexcitation from a grating monochromator was focused to a 1 mm-diameter spot, with optical flux 3×10^{15} to 2×10^{12} photons/cm^2 sec at 1000 and 350 nm, respectively. Photoconductivity (10 Hz chopping rate) was measured at 293 K and 120 V (4×10^4 V/cm).

Recall that band tails in inorganic material are typically observed using optical absorption or photoconductivity, with crystals [6,7] having narrow, temperature-dependent, band tails (Urbach tails) given by $\sim \exp[-(E_g - E)/nkT]$, where E_g is the band gap, E is the photon energy, k is Boltzmann's constant, T is the absolute temperature, and $n \sim 1$, and amorphous materials [7] typically having broader, temperature-independent, band tails, given by $\sim \exp[-\beta(E_g - E)]$, with the slope parameter β in the range 10 to 25 eV^{-1} at 300 K. Band tails in organic materials are usually not measurable by these methods because exciton effects often dominate the absorption spectrum within about 0.2–0.4 eV of the intrinsic highest occupied molecular orbital–lowest unoccupied molecular orbital (HOMO-LUMO) gap [8]. Therefore, we must compare a variety of optical measurements in this spectral region to distinguish the exciton effects from the absorption due to the localized band-tail states. Figure 1 shows our photocurrent yield spectrum along with that of Silinsh *et al.* [9],

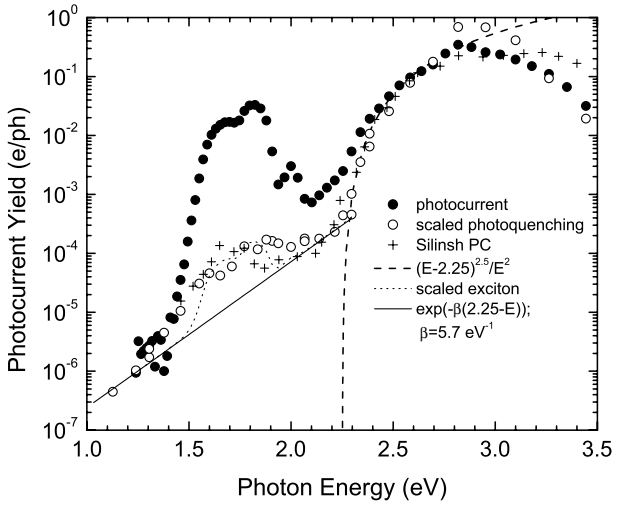

FIG. 1. Photocurrent yield (electrons/photon) for single-crystal pentacene versus photon energy. The photoquenching rate of the metastable hole trap is normalized to the photocurrent above 2.2 eV. The photocurrent yield data of Silinsh *et al.* is plotted without adjustable parameters. Various fits to the data are described in the text.

which agrees remarkable well above the 2.2 eV HOMO-LUMO gap (no adjustable parameters), but is dramatically different in the range 1.5 to 2.2 eV. Both samples were purified by two- or threefold vacuum sublimation before the final growth, so it is unlikely that the spectral differences are due to impurities. We believe the variations are due to different decay paths for excitons in our crystals compared to polycrystalline films. To explain these effects we need to briefly review some pertinent facts about excitons in organic materials.

Excitons in organic materials play a complex role in photoconductivity [8–10] compared to inorganic materials where they typically contribute directly at room temperature as electrons and holes separated by thermal excitation and electric fields. The large exciton binding energies in organics effectively eliminate direct dissociation under most conditions so that excitons must follow a more complex series of decay paths to create photoconductivity. In pentacene the singlet excitons at 1.82 and 1.94 eV dominate the optical absorption spectrum [9,11,12] and rapidly decay with a rate of 1.3×10^{13} sec^{-1} into pairs of $\sim$0.8 eV triplet excitons [13]. The optical decay of triplet excitons is forbidden by selection rules, leaving nonradiative decay paths such as interacting with paramagnetic molecules [14], free carriers [14], or trapped carriers [9,10]. The photocurrent yield therefore depends on the relative strengths of the triplet decay paths that emit trapped carriers versus those that emit only vibrational energy. Photoconductivity in the spectral range of the singlet exciton is due both to the direct excitation of carriers from localized gap states as well as the release of trapped carriers by triplet excitons, with the ratio depending on the types and concentrations of defects. The photocurrent yield at 1.8 eV in our pentacene single crystals is 250 times stronger than in the polycrystalline films of Silinsh *et al.* This could be due either to stronger triplet-exciton–trapped-carrier interactions in our crystals or stronger triplet-exciton quenching interactions in Silinsh's samples, with the latter situation being more likely in polycrystalline material. Note that both of these samples have the same photocurrent yield below 1.5 and above 2.3 eV where exciton effects are less important.

We also show in Fig. 1 the spectrum of the photoquenching rate of the defect generation process we recently discovered in pentacene [15]. In this process a bias stress applied to the sample in the dark slowly generates a defect with a localized state 0.38 eV above the valence band. Subsequent exposure to light removes this defect at a rate that is dependent on the wavelength and intensity of the light. The presence of this defect state is observed by its effect on space-charge-limited current (SCLC). The photoquenching data in Fig. 1 are obtained in the following manner. The sample is first stressed at a bias of 600 V (2×10^5 V/cm) for 100 sec at 291–293 K to create the defects. It is then measured at 120 V to observe the rate of photoinduced reduction in the defect concentration via changes in the SCLC. Under these conditions, the thermally activated decay of the defect concentration in the dark is negligible [15]. However, under illumination the SCLC decays to its prestress value in 1–100 sec, depending on the wavelength and intensity of the light. This sequence is repeated for various wavelengths to obtain the photoquenching spectrum in Fig. 1 from the inverse of the time constant of the SCLC decay normalized by the photon flux. The scale factor that relates the photoquenching effect to photocurrent yield is not known, thus the photoquenching data are scaled to fit the photocurrent yield data above 2.3 eV.

The HOMO-LUMO absorption edge in Fig. 1 is fit with the function $(E\text{-}E_g)^n/E^2$ with $n = 2.5$ and $E_g = 2.25$ eV; this power law with $n = 2$ is typical of the optical absorption edge in many amorphous solids [7]. Silinsh *et al.* [9] originally fit their data to the function $(E\text{-}E_g)^{5/2}$ with $E_g = 2.20$ eV; this power law is typical of the photoconductivity threshold in many organic crystals [8]. The fact that the optical spectra in Fig. 1 have the same shape above the HOMO-LUMO gap indicates that all three processes probe the intrinsic rate of carrier photogeneration. As mentioned above, the differences below 2.25 eV are due to variations in the ratio of the indirect exciton processes to the direct photogeneration rate of carriers from localized gap states. The detailed mechanism for the photoquenching of the bias-stress generated defects is presently unknown, but the similarity of the three spectra above 2.25 eV indicates that the process is proportional to the intrinsic rate of carrier photogeneration. Since the

photocurrent is primarily due to holes [9], the fact that the photoquenching rate falls off faster than the photocurrent below 2.25 eV in our crystals implies that the photoquenching process is dominated by the capture of electrons at the bias-stress generated defects. The dominance of electron capture in the photoquenching process is reasonable since the bias-stress defects are generated when the Fermi level is closer to the valence band than 0.4 eV and decay when the Fermi level is above 0.4 eV. Thus the capture of photogenerated electrons by this defect moves the Fermi level higher in the gap and also provides approximately 1.9 eV in capture energy from the conduction band into the 0.38 eV defect level, which could be channeled into a defect reaction coordinate [16]. Therefore we believe that the photoquenching spectrum is a good measure of the true band tails of the material with only a small exciton effect.

The photoquenching data, along with the data of Silinsh *et al.* [9], define an exponential band tail with a slope of $\beta = 5.7\ \mathrm{eV}^{-1}$ plus a 0.3 eV-wide peak centered at 1.75 eV, as shown in Fig. 1. The 1.75 eV peak is in the spectral region usually identified as due to singlet exciton absorption. The dotted line labeled "scaled exciton" is a fit that is equal to our photocurrent data in this spectral region multiplied by 0.004 and added to the exponential tail function with $\beta = 5.7\ \mathrm{eV}^{-1}$. We believe this band tail is a good measure of the bulk gap states in pentacene. Since both of the samples in Fig. 1 were purified by two- or threefold vacuum sublimation before the final growth, we believe these band tails are most likely due to disorder rather than impurities.

We will now extract the density-of-gap states from our FET data [5] shown in Fig. 2(a), which gives the activation energy of the source-drain current at 40 V as a function of the gate bias in the temperature range of 200–300 K. The density-of-gap states, $N(E)$, can be obtained from these data in the limit where the concentration of free carriers is much less than the concentration of trapped carriers by assuming that the charge induced by the gate bias is nearly all trapped. The charge per unit area induced in the FET by a gate bias V_g is given by $Q = CV_g$, where C is the gate capacitance per unit area. The area density of states, $N(E)$ in states/cm^2 eV, is given by $N(E) = (C/q)[1/(dE/dV_g)]$, where q is the electronic charge and E is the energy measured from the valence-band edge; E is also approximately equal to the activation energy in Fig. 2(a). The gate capacitance for our device [5] is $C = 6 \times 10^{-9}\ \mathrm{F/cm}^2$. The area density of states can be converted into a volume density by determining the depth over which the carriers are trapped, which Völkel *et al.* [4] determined to be within 5–10 nm of the interface.

Figure 2(b) gives $N(E)$ obtained from the smooth fit to the data in Fig. 2(a) with a trapping depth of 7.5 nm. The best fit to these data is a peak at 0.35 eV plus an exponential band tail $N_0 \exp(-\beta E)$, with $N_0 = 9 \times 10^{19}\ \mathrm{cm}^{-3}\mathrm{eV}^{-1}$ and $\beta = 9.2\ \mathrm{eV}^{-1}$. The density-of-states functions obtained by Völkel *et al.* [4] for donor and acceptor defects are shown in Fig. 2(b) for comparison. The similarity between polycrystalline TFTs and a single-crystal FET suggests that the density of defects near the gate interface is similar in both cases. In both cases the effective mobilities are also very similar: 0.3 cm^2/V sec for the single-crystal device [5] and 0.3 to 0.6 cm^2/V sec for the polycrystalline TFTs [4]. Note that the peak at 0.35 eV is the same within experimental error as the gap state at 0.38 eV due to the defects created by bias stress in pentacene [15].

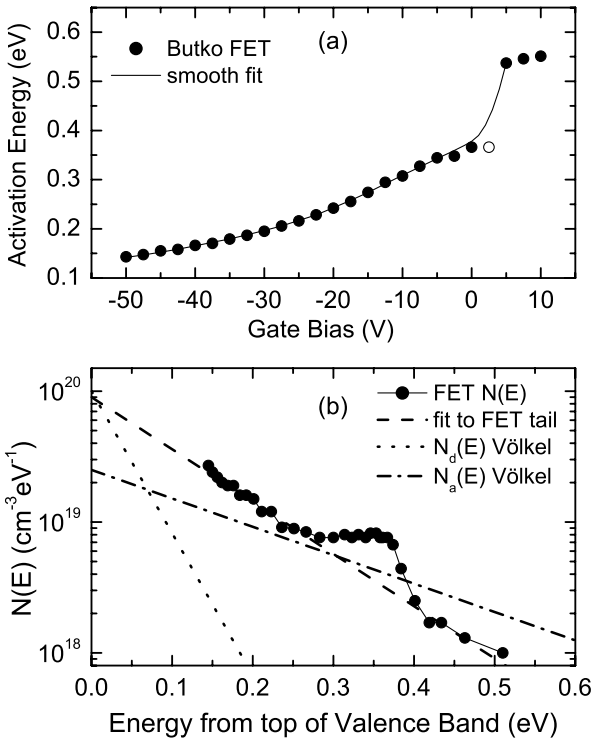

FIG. 2. (a) FET data of Butko *et al.* with a smooth fit to the data as described in the text. (b) Density of states, $N(E)$, obtained from the FET data in part (a) of this figure using a trapping depth of 7.5 nm. The band tails of Völkel *et al.* and the fit to the FET band tail are described in the text.

Figure 3 shows both the optical data from Fig. 1 and the FET data from Fig. 2(b) on the same density-of-states scale with the energy measured from the top of the valence band. The density-of-states scale for the optical data is determined as follows: Both the upper valence band and lower conduction band in pentacene have roughly a 0.5 eV width [12]. The number of states in one of these bands is of the order of one state per molecule, so the density of states at the maximum is roughly the molecular density of pentacene ($2.9 \times 10^{21}\ \mathrm{cm}^{-3}$) divided by the width of the band ($\sim$0.5 eV), or $5.8 \times 10^{21}\ \mathrm{cm}^{-3}\,\mathrm{eV}^{-1}$. We can therefore roughly convert the photoconductivity data in Fig. 1 into a density of states

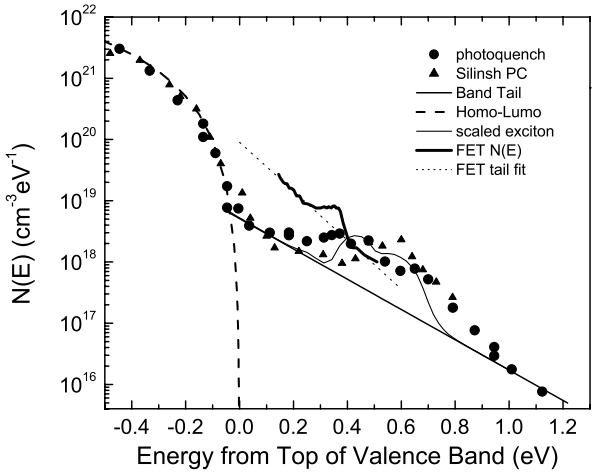

FIG. 3. Photoquenching rate and Silinsh photocurrent yield normalized to a density-of-states scale as described in the text. The FET density of state is from Fig. 2(b). The FET and optical band tails are given as a function of energy measured from the top of the valence band. The HOMO-LUMO curve is the photocurrent threshold line shape function given in Fig. 1.

by normalizing the peak of the band-to-band photocurrent yield (at ~2.8 eV) to this maximum value, as shown in Fig. 3. Note that the FET band tail is significantly larger than the optical band tail. Since the FET data correspond to traps within 5–10 nm of the parylene gate dielectric, these results imply that such defects or impurities are either introduced by the parylene deposition process or exist near the surface of the crystal before the gate fabrication.

The origins of the bulk and interface band tails in pentacene are presently unknown; however, we can consider some possible causes. Calculations have shown that lattice relaxation near a point defect in anthracene could create a 0.28 eV trap level and the strain field near a dislocation could give a 0.2 eV trap [8,17]. Various hydrogen- and oxygen-induced defects in crystalline pentacene are quite likely to be in the starting material and create hole traps at 0.34 and 0.18 eV from the valence band [18]. It is also possible that defects and/or impurities could be introduced into the sample after it is grown by either exposure to the atmosphere or by the contact or gate dielectric deposition process. Clearly, there are many opportunities to improve the material for enhanced device performance.

In conclusion, we have shown that purified pentacene single crystals still have sufficient disorder and/or impurities to have substantial band tails, even broader than the band tails observed in inorganic amorphous solids. In addition, FET devices fabricated from pentacene single crystals and polycrystalline thin films can have an order of magnitude more valence-band-tail states within 5–10 nm of the gate dielectric than is typical of bulk pentacene in these two forms. This suggests that devices can be substantially improved by reducing these interface-related states to the bulk concentration level or below.

We acknowledge the support of the U.S. Department of Energy under Grant No. 04SCPE389. This work was partially supported by the Nanoscale Science and Engineering Initiative of the National Science Foundation under NSF Grant No. CHE-0117752 and by the New York State Office of Science, Technology, and Academic Research (NYSTAR).

[1] S. Forrest, P. Burrows, and M. Thompson, IEEE Spectrum **37**, 29 (2000); C. D. Dimitrakoupolis and D. J. Mascaro, IBM J. Res. Dev. **45**, 11 (2001); C. D. Dimitrakopoulos and P. R. L. Malenfant, Adv. Mater. **14**, 99 (2002).
[2] I. H. Campbell and D. L. Smith, in *Solid State Physics* (Academic Press, San Diego, 2001), Vol. 55, p. 1.
[3] N. Karl, K. H. Kraft, J. Marktanner, M. Munch, F. Schatz, R. Stehle, and H. M. Uhde, J. Vac. Sci. Technol. A **17**, 2318 (1999).
[4] A. R. Völkel, R. A. Street, and D. Knipp, Phys. Rev. B **66**, 195336 (2002).
[5] V. Y. Butko, X. Chi, D. V. Lang, and A. P. Ramirez, Appl. Phys. Lett. **83**, 4773 (2003).
[6] J. I. Pankove, *Optical Processes in Semiconductors* (Prentice-Hall, Englewood Cliffs, NJ, 1971).
[7] G. A. N. Connell, in *Amorphous Semiconductors*, edited by M. H. Brodsky (Springer, New York, 1979), Vol. 36, p. 71.
[8] M. Pope and C. E. Swenberg, *Electronic Processes in Organic Crystals and Polymers* (Oxford, New York, 1999).
[9] E. A. Silinsh, A. I. Belkind, D. R. Balode, A. J. Biseniece, V. V. Grechov, L. F. Taure, M. V. Kurik, J. I. Vertzmacha, and I. Bok, Phys. Status Solidi (a) **25**, 339 (1974).
[10] G. Jarosz, R. Signerski, and J. Godlewski, Adv. Mater. Opt. Electron. **6**, 379 (1996).
[11] S. P. Park, S. S. Kim, J. H. Kim, C. N. Whang, S. Im, S. S. Kim, Y. S. Choi, K. Kim, J. H. Kim, and S. Im, Appl. Phys. Lett. **80**, 2872 (2002); S. S. Kim *et al.*, Appl. Phys. Lett. **82**, 639 (2003).
[12] M. L. Tiago, J. E. Northrup, and S. G. Louie, Phys. Rev. B **67**, 115212 (2003).
[13] C. Jundt, G. Klein, B. Sipp, J. LeMoigne, M. Joucla, and A. A. Villaeys, Chem. Phys. Lett. **241**, 84 (1995).
[14] W. Helfrich, Phys. Rev. Lett. **16**, 401 (1966).
[15] D. V. Lang, X. Chi, T. Siegrist, A. M. Sergent, and A. P. Ramirez, Phys. Rev. Lett. **93**, 076601 (2004).
[16] D. V. Lang, Annu. Rev. Mater. Sci. **12**, 377 (1982).
[17] J. Sworakowski, Mol. Cryst. Liq. Cryst. **33**, 83 (1976).
[18] J. E. Northrup and M. L. Chabinyc, Phys. Rev. B **68**, 041202 (2003).